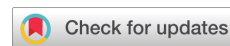


Received 16 May 2023; Accepted 7 July 2023
<https://doi.org/10.22226/2410-3535-2023-4-308-311>



Effect of high-pressure torsion on mechanical properties and *in vitro* biocompatibility of pure Zn

N. S. Martynenko^{†,1}, N. Yu. Anisimova^{1,2,3}, N. Yu. Tabachkova^{3,4}, V. N. Serebryany¹,
 O. V. Rybalchenko¹, A. V. Sannikov^{1,3}, D. R. Temralieva¹, E. A. Lukyanova¹,
 E. A. Kornjushenkov², M. V. Kiselevskiy^{2,3}, S. V. Dobatkin¹

[†]nataliasmartynenko@gmail.com

¹A. A. Baikov Institute of Metallurgy and Materials Science of the RAS, Moscow, 119334, Russia

²N. N. Blokhin National Medical Research Center of Oncology of the Ministry of Health of the Russian Federation, (N. N. Blokhin NMRCO), Moscow, 115478, Russia

³National University of Science and Technology "MISIS", Moscow, 119049, Russia

⁴A. M. Prokhorov General Physics Institute of the RAS, Moscow, 119991, Russia

Abstract: Effect of the structure and texture caused by high pressure torsion (HPT) on mechanical properties, corrosion resistance and *in vitro* biocompatibility of pure Zn was studied. HPT leads to the formation of an ultrafine-grained (UFG) structure with an average grain size of 710 ± 40 nm. In addition, a sharp basal texture is formed in pure Zn after HPT. These structure and texture features lead to an increase in the ultimate tensile strength of pure Zn by 5.5 times while the ductility grows significantly. Pure Zn in both microstructural states does not increase the hemolytic activity of red blood cells. An interesting observation is the reduction of the cytotoxicity of pure Zn after HPT, which can be associated with a slight increase in its degradation rate.

Keywords: zinc, high pressure torsion, microstructure, mechanical properties, degradation, biocompatibility *in vitro*

1. Introduction

Zinc and its alloys are promising medical materials [1,2]. Their use in medicine is due to good biocompatibility [3], antibacterial [4,5], osteogenic properties [6], etc. However, the practical application of as-cast Zn in osteosynthesis is limited by its poor mechanical properties [7]. Wang et al. showed that the ultimate tensile strength of as-cast pure Zn is 33.94 MPa with the ductility level 3% [8]. The application of deformation processing is an efficient way to improve the mechanical characteristics of pure Zn. At the same time, the severe plastic deformation (SPD) methods provide an effective way to increase the strength of materials without losing their corrosion resistance, which is an important operational property of medical materials [5,9]. There are a number of works devoted to studying the effect of SPD on the behavior of pure zinc and its alloys developed for medical applications [5,10–13]. Bednarczyk et al. showed that deformation of pure Zn by equal channel angular pressing (ECAP) method at room temperature led to an increase in its strength and ductility [9]. Srinivasarao et al. studied the effect of different numbers of turns (N) of high-pressure torsion (HPT) on mechanical properties of pure Zn [13]. They showed that HPT ($N=5$) of pure Zn also caused an increase in the strength (≈ 150 MPa) and ductility ($\approx 24\%$) because of grain refinement and sharp basal texture formation. Polenok et al. also deformed pure Zn by 10 turns of HPT under the pressure of 2 GPa and showed the possibility

of its strengthening up to 130 MPa [14]. This shows that HPT is a promising method for the development of high-strength zinc alloys with an increased ductility. However, it is important to study not only mechanical characteristics, but also the corrosion resistance and biocompatibility after deformation. Therefore, the study of effect of HPT on the mechanical and corrosion properties and biocompatibility *in vitro* of pure Zn was the aim of this work.

2. Materials and experimental methods

Pure Zn (99.975 wt.%) melted in an induction furnace in air condition was studied. Disks 20 mm in diameter and 1.5 mm in thickness were cut from an ingot to conduct HPT. HPT was carried out at the room temperature under a pressure of 4 GPa up to the number of turns $N=10$. The microstructure of as-cast Zn was studied using an optical microscope Axio Observer D1m Carl Zeiss. A JEM-2100 (JEOL) electron microscope operating at a voltage of 200 kV was used to study the microstructure after HPT. The microhardness was measured on a 402 MVD Instron Wolpert Wilson Instruments microhardness tester. The mechanical properties were determined on an Instron 3382 testing machine at room temperature on flat samples with a cross-sectional area of 2×1 mm and a working length of 5.75 mm. The texture was studied on a DRON-7 X-ray texture diffractometer using the CuK_α radiation in the reflection mode. Five incomplete pole figures $\{00.2\}$, $\{10.0\}$, $\{10.1\}$, $\{10.2\}$, $\{11.0\}$ were recorded at

the maximum inclination angle $\alpha_{\max} = 70^\circ$ with a step of 5° for α and β angles ($0 - 360^\circ$) (α and β are the radial and azimuth angles on the pole figure). The orientation distribution function (ODF) and the orientation factors were calculated as described in [15] and [16]. The degradation rate was assessed by the immersion method in a solution based on DMEM (Dulbecco's modified Eagles medium). The studies were carried out at a temperature of 37°C for 8 days [17]. The biocompatibility *in vitro* was assessed by the study of hemolysis of red blood cells (RBC) and cytotoxicity of mononuclear leucocytes (ML). Hemolysis and ML viability were assessed as described earlier in [18]. Cells incubated in the complete growth medium without alloys under the same conditions were used as a control.

3. Results and discussion

Figure 1 shows the results of microstructure studies of pure Zn before and after HPT. The structure of as-cast zinc consists of irregularly shaped grains with a size of about $70 - 100 \mu\text{m}$. A significant grain refinement with the formation of grains with a size of $710 \pm 40 \text{ nm}$ occurs after HPT. Grains after HPT have clear boundaries with mostly high-angle misorientations. The presence of high-angle boundaries is also indicated by the absence of diffuse reflections in the ring electron diffraction pattern.

It is known that the strain during HPT depends on the distance from the sample center [19]. The strain grows with the distance from the center of the sample, which leads to the formation of heterogeneity of the structure and properties. The studies of microhardness after HPT showed that it had a fairly uniform distribution over the sample diameter (Fig. 2 a). A slight decrease is observed in the center of samples, where the strain has the minimal value. It should be noted that the microhardness after HPT increases insignificantly from $553 \pm 18 \text{ MPa}$ in the center of the sample to $587 \pm 26 \text{ MPa}$ on a distance of a half-radius from it. Taking into account the obtained results, samples for tensile tests were cut out from the zone corresponding to the half of the disk radius.

Figure 2b and Table 1 show the results of the tensile tests. The yield stress (YS) of pure Zn is $41 \pm 8 \text{ MPa}$, while the ultimate tensile strength (UTS) is $44 \pm 7 \text{ MPa}$. Grain refinement caused by HPT increases these characteristics up to $218 \pm 4 \text{ MPa}$ and $247 \pm 12 \text{ MPa}$, respectively. It should be noted that an increase in ductility (El) from $6.2 \pm 1.3\%$ to $55.1 \pm 14.4\%$ is also observed after HPT.

Table 1. The mechanical characteristics of pure Zn.

Processing	YS, MPa	UTS, MPa	El, %
As-cast state	41 ± 8	44 ± 7	6.2 ± 1.3
HPT	218 ± 4	247 ± 12	55.1 ± 14.4

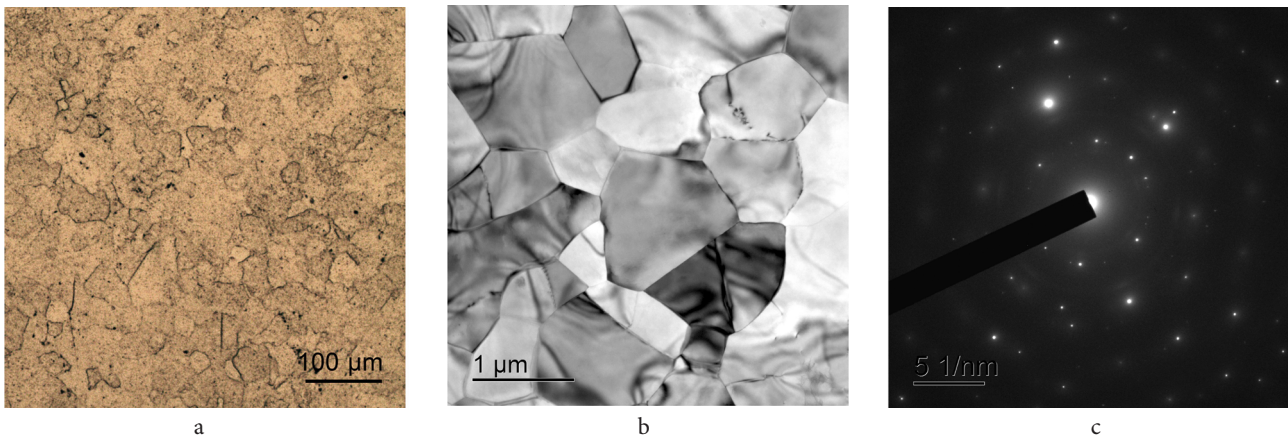


Fig. 1. (Color online) The structure of pure Zn in the as-cast state (a) and after HPT (b) with SAD pattern (c).

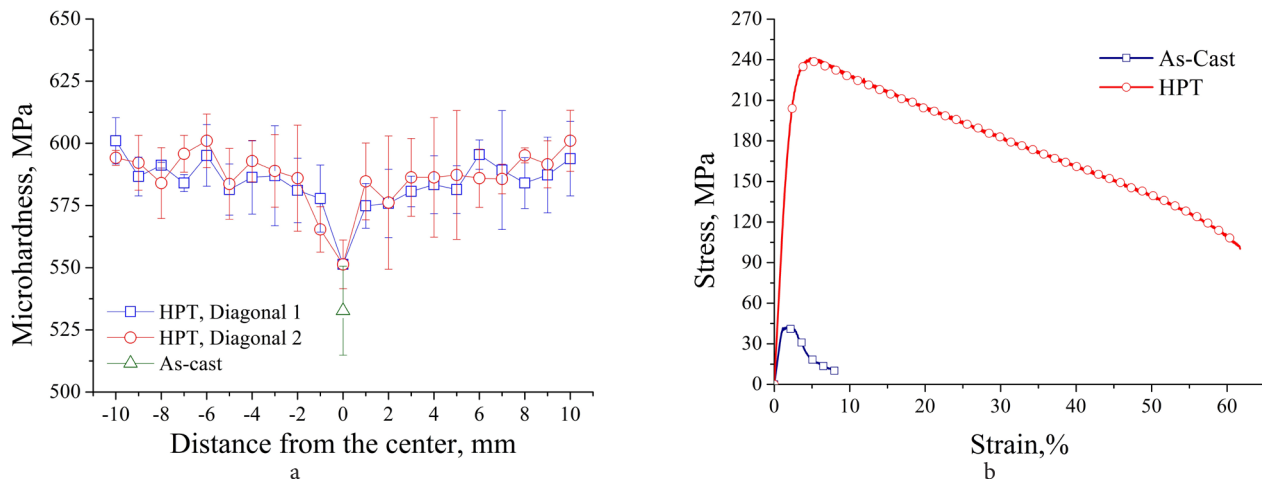


Fig. 2. (Color online) Distribution of microhardness over the diameter of the sample after HPT (a) and engineering stress - strain response of pure Zn in both conditions (b).

Figure 3 shows the results of texture measurements in pure Zn in the as-cast state and after HPT. The texture of as-cast Zn is characterized by a disperse basal orientation. A sharp basal texture is formed after HPT due to the activation of basal slip as the main mechanism of deformation of zinc during HPT.

Table 2 shows the values of the orientation factors (the reciprocals of Schmid factors) of the main deformation systems in Zn. They confirm the thesis about the activation of basal slip as one of the main mechanisms of zinc deformation during HPT. The decrease in the value of the orientation factor for pyramidal slip systems is also an indication of their activation. The growth of ductility can be associated with these texture features. Ye at al. showed that the ductility of the Zn-0.1%Mg alloy after equal-channel angular pressing increased by more than 45% due to an activation of pyramidal slip [20]. We also obtained similar results on Zn-1%Mg [21] and Zn-1%Mg-0.1%Ca [18] alloys after HPT.

Table 2. Orientation factors for pure Zn in the as-cast state and after HPT.

Processing	Basal {0001} <110>	Prismatic {100} <110>	Pyramidal {112} <113>
As-cast state	4.83	6.87	4.28
HPT	8.11	17.60	2.83

Table 3 shows the results of study of degradation rate, RBC hemolysis and ML viability in comparison with Control.

The analysis of the data shows that pure Zn in both as-cast and HPT-treated states does not demonstrate a significant hemolytic activity. At the same time, pure Zn in the as-cast state significantly inhibits the ML viability. However, coincubation of pure Zn treated by HPT with MLs does not cause a significant decrease in their viability in comparison with Control. At the same time, a significant increase in viability of MLs is observed compared to as-cast Zn. The increase in viability of MLs can be associated with a slight increase in the degradation rate of pure Zn after HPT from 0.15 ± 0.02 to 0.21 ± 0.03 mm/y. It is obvious that an increase in the degradation rate leads to an increase in the concentration of Zn^{2+} ions. It was shown that an increase in the concentration of Zn^{2+} ions decreased the cytotoxicity of Zn^{2+} functionalized hydroxyapatite composite [22]. It was also shown that Zn^{2+} ions had an interesting effect: low concentrations promote cell adhesion and proliferation, while high concentrations cause opposite cellular responses [23]. Therefore, the study of this phenomenon is still an important task.

4. Conclusions

1. HPT of pure Zn leads to the grain refinement from 70–100 μm in the as-cast state to 710 ± 40 nm after deformation.

Table 3. Biocompatibility parameters and biodegradation rate of pure Zn in various states.

Parameter	Condition	Mean ± SD, %	*p	**p
Hemolysis	As-cast	110 ± 27	0.74	0.9
	HPT	114 ± 0	0.26	
	Control	100 ± 1	-	-
ML viability	As-cast	74 ± 1	0.002	0.03
	HPT	84 ± 2	0.11	
	Control	100 ± 7	-	-
Degradation rate	Annealing	0.15 ± 0.02	-	0.19
	HPT	0.21 ± 0.03	-	

*difference from control

**difference between as-cast and HPT-treated states

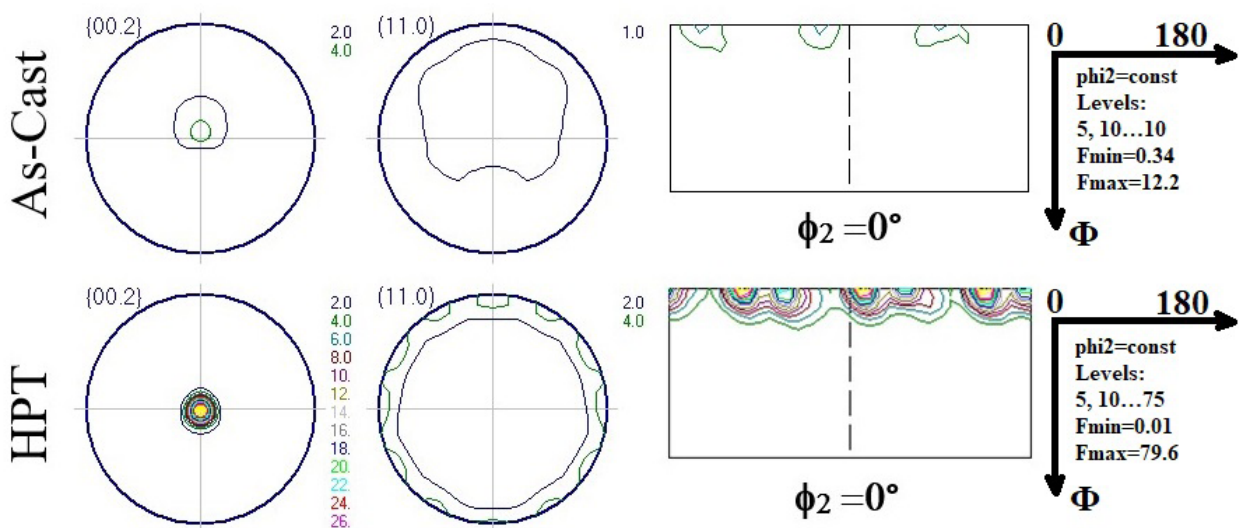


Fig. 3. (Color online) {00.2} and {11.0} pole figures and ODF sections at $\phi_2 = 0^\circ$ for pure Zn before and after HPT.

2. The grain refinement increases the strength (YS — from 41 ± 8 to 218 ± 4 MPa, UTS — from 44 ± 7 to 247 ± 12 MPa) and ductility (from $6.2 \pm 1.3\%$ to $55.1 \pm 14.4\%$) of pure Zn.

3. HPT of pure Zn leads to the formation of a sharp basal texture.

4. HPT does not affect the hemolytic activity, but reduces the ML cytotoxicity of pure Zn compared to as-cast state due to a slight increase in its degradation rate.

Acknowledgments: This research was funded through Russian Science Foundation (Grant #22-23-00097).

References

1. W. Yuan, D. Xia, S. Wu, Y. Zheng, Z. Guan, J.V. Rau. *Bioact. Mater.* 7, 192 (2022). [Crossref](#)
2. X. Zhu, T. Ren, P. Guo, L. Yang, Y. Shi, W. Sun, Z. Song. *Mater. Today Commun.* 31, 103639 (2022). [Crossref](#)
3. X. Tong, L. Zhu, K. Wang, Z. Shi, S. Huang, Y. Li, J. Ma, C. Wen, J. Lin. *Acta Biomater.* 142, 361 (2022). [Crossref](#)
4. C. García-Mintegui, L.C. Córdoba, J. Buxadera-Palomero, A. Marquina, E. Jiménez-Piqué, M.-P. Ginebra, J.L. Cortina, M. Pegueroles. *Bioact. Mater.* 6 (12), 4430 (2021). [Crossref](#)
5. C. García-Mintegui, I. Goncharov, L. Ortiz-Membrado, E. Jiménez-Piqué, M.-P. Ginebra, M. Vedani, J. L. Cortina, M. Pegueroles. *Mater. Des.* 228, 111817 (2023). [Crossref](#)
6. B. Jia, H. Yang, Z. Zhang, X. Qu, X. Jia, Q. Wu, Y. Han, Y. Zheng, K. Dai. *Bioact. Mater.* 6 (6), 1588 (2021). [Crossref](#)
7. H. F. Li, X. H. Xie, Y. F. Zheng, Y. Cong, F. Y. Zhou, K. J. Qiu, X. Wang, S. H. Chen, L. Huang, L. Tian, L. Qin. *Sci. Rep.* 5, 10719 (2015). [Crossref](#)
8. C. Wang, Y. Hu, C. Zhong, C. Lan, W. Li, X. Wang. *Mater. Sci. Eng. A.* 846, 143276 (2022). [Crossref](#)
9. N. Martyntenko, E. Lukyanova, N. Anisimova, M. Kiselevskiy, V. Serebryany, N. Yurchenko, G. Raab, N. Birbilis, G. Salishchev, S. Dobatkin, Y. Estrin. *Materialia.* 13, 100841 (2020). [Crossref](#)
10. W. Bednarczyk, M. Wątroba, J. Kawałko, P. Bała. *Mater. Sci. Eng. A.* 748, 357 (2019). [Crossref](#)
11. H. Huang, H. Liu, L.-S. Wang, Y.-H. Li, S.-O. Agbedor, J. Bai, F. Xue, J.-H. Jiang. *Acta Metall. Sin-Engl.* 33, 1191 (2020). [Crossref](#)
12. L. Ye, C. Sun, X. Zhuo, H. Liu, J. Ju, F. Xue, J. Bai, J. Jiang, Y. Xin. *J. Alloys Compd.* 919, 165871 (2022). [Crossref](#)
13. B. Srinivasarao, A. P. Zhilyaev, T. G. Langdon, M. T. Pérez-Prado. *Mater. Sci. Eng. A.* 562, 196 (2013). [Crossref](#)
14. M. V. Polenok, E. D. Khafizova, R. K. Islamgaliev. *Frontier Materials & Technologies.* 3–2, 25 (2022). (in Russian) [Crossref](#)
15. T.I. Savyolova, S.F. Kourtasov. *Mater. Sci. Forum,* 459–457, 301 (2005). [Crossref](#)
16. V.N. Serebryany, L.L. Rokhlin, A.N. Monina. *Inorg. Mater. Appl. Res.* 5 (2), 116 (2014). [Crossref](#)
17. ASTM G31–21, Standard guide for laboratory immersion corrosion testing of metals, ASTM International, West Conshohocken, PA, ASTM International (2004).
18. N. Martyntenko, N. Anisimova, O. Rybalchenko, M. Kiselevskiy, G. Rybalchenko, N. Tabachkova, M. Zheleznyi, D. Prosvirnin, D. Filonenko, V. Bazhenov, A. Koltygin, V. Belov, S. Dobatkin. *Metals.* 12 (10), 1681 (2022). [Crossref](#)
19. A. P. Zhilyaev, T. G. Langdon. *Prog. Mater. Sci.* 53, 893 (2008). [Crossref](#)
20. L. Ye, H. Liu, C. Sun, X. Zhuo, J. Ju, F. Xue, J. Bai, J. Jiang, Y. Xin. *J. Alloys Compd.* 926, 166906 (2022). [Crossref](#)
21. N. Martyntenko, N. Anisimova, O. Rybalchenko, M. Kiselevskiy, G. Rybalchenko, N. Tabachkova, M. Zheleznyi, D. Temralieva, V. Bazhenov, A. Koltygin, A. Sannikov, S. Dobatkin. *Materials.* 15 (24), 9073 (2022). [Crossref](#)
22. A. Bhattacharjee, S. Bose. *Mater. Des.* 221, 110903 (2022). [Crossref](#)
23. J. Ma, N. Zhao, D. Zhu. *Sci. Rep.* 6, 2666 (2016). [Crossref](#)